Nonequilibrium behavior of thin polymer films

Katherine R. Thomas,[1] Alexis Chenneviere,[1,*] Günter Reiter,[2,3] and Ullrich Steiner[1,2,†]
[1]*Cavendish Laboratory, University of Cambridge, Cambridge CB3 0HE, United Kingdom*
[2]*Freiburg Institute for Advanced Studies, Albert-Ludwigs-Universität, D-79104, Freiburg, Germany*
[3]*Albert-Ludwigs-Universität Physikalisches Institut, D-79104, Freiburg, Germany*
(Received 9 November 2010; published 28 February 2011)

The rheological behavior of 100-nm-thick polystyrene films cast from various solvents was examined using an electric field to weakly perturb the free surface of the polymer melt. The effective viscosity and residual stresses of the as-spun films are seen to strongly depend on the properties of the casting solvent and the solvent quality. Both effects are explained in terms of the coil dimension at the solvent-polymer composition at which the film vitrifies. The more compact chains in a near-Θ-solvent are less entangled and less deformed when quenched to the dry melt compared to the more swollen chains in an athermal solution. Despite chain conformations that are further from equilibrium for the Θ-solvent cast chains, these films have reduced stored stresses compared to the chains cast in films from athermal solvents. A more detailed analysis of the data suggests that the formation of a surface-near region with more strongly deformed chains during spin coating. Since thermal equilibration of spin-cast high-molecular-weight films is unpractical, solvent vapor annealing was used to equilibrate films on timescale of a few hours.

DOI: 10.1103/PhysRevE.83.021804 PACS number(s): 61.41.+e, 68.60.−p, 83.60.Np, 83.50.−v

I. INTRODUCTION

Film formation via spin coating is widely used in polymer science and is important in many technological processes. The popularity of this technique stems from the ability to form uniform films over large areas with a well-defined thickness. While sufficiently ($\gtrsim$100 nm) thick spin-cast films are commonly thought to be bulklike, very thin films often exhibit anomalous structural and dynamic properties [1–12]. In some instances very thin spin-cast films can be equilibrated by thermal annealing above the glass transition temperature T_g of the polymer, restoring bulk behavior [13–16].

The difference in behavior observed between as-cast and annealed films may arise from nonequilibrium conformations of the polymer chains and residual stresses resulting from the preparation of the films from solutions by rapid solvent evaporation [17]. These nonequilibrium chain conformations can give rise to changes in the viscoelastic properties of the samples [18]. A number of different groups have shown experimentally that the viscosity of as-cast films is significantly reduced compared to the bulk [7,14,17].

The behavior of thin polymer films is commonly studied using dewetting experiments [19]. Residual stresses stored in the films provide an additional driving force for the dewetting, thereby accelerating the process [20]. When the films are aged above T_g, these stresses are seen to relax and the hole growth slows down [21]. For films aged below T_g a decreasing number of spontaneously nucleated holes per unit area are observed upon heating above T_g [22]. This leads to the projection that no heterogeneously nucleated holes will form in an idealized polymer film aged for a sufficiently long time period.

Recent work by Raegen *et al.* suggests that the quality of casting solvent has a strong influence on the behavior of spin-cast films [23]. The characteristic aging time was seen to vary strongly with the quality of the solvent that the film was cast from. This was attributed to a variation in the frozen-in distortion of chain conformations in as-cast films. These results suggest that the anomalous behavior observed in as-cast films originates from the preparation of the films and can be removed through aging.

While dewetting experiments provide insight into the nonequilibrium properties of as-cast films, fully equilibrated films cannot be investigated due to the intrinsically unstable nature of the films. Barbero *et al.* have shown that electric fields can be used to perturb the free surface of a polymer films, heated above T_g, in order to probe the rheology of liquid films [7]. In these experiments liquid films that are stable in the absence of the electric field can be used, allowing the direct comparison of as-cast and fully equilibrated films.

The present study systematically investigates the role of the spin-coating solvent on the nonequilibrium behavior of 100-nm-thick polystyrene (PS) films. The electrohydrodynamic (EHD) destabilization of the thin films probes the viscosity and residual stress in the films. Particular attention is paid to the annealing times required to restore bulk behavior.

II. EXPERIMENT

Polystyrenes (PSs) of three molecular weights were used: $M_w = 200$ kg mol^{-1} (PS200), $M_w/M_n = 1.09$ (Polymer Source), $M_w = 655$ kg mol^{-1} (PS655), $M_w/M_n = 1.09$ (Polymer Source), and $M_w = 4000$ kg mol^{-1} (PS4000), $M_w/M_n = 1.15$ (Polymer Standards Service) were used as obtained. PS films were spin-coated onto cleaned silicon substrates, from solution, with a spin speed of 4500 rpm. The solvents used and their properties are given in Table I. Films spun from trans-decalin (TD) solutions were spun at 25 °C (TD25) and 55 °C (TD55). TD solutions were heated in a water bath, while the spin-coater chuck was heated using an incandescent lamp. A thermal couple placed on the chuck reached equilibrium at the same temperature as the solution. Care was taken to minimize the thermal variation during the spin coating process,

*Also at: Ecole Polytechnique, Paris
†u.steiner@phy.cam.ac.uk

TABLE I. Boiling point T_{bp}, melting point T_m, and volume fraction of solvent ϕ_g at vitrification of the polymer at 25 °C (55 °C for TD55) of the spin-coating solvents, from Ref. [24]. R_c is the coil radius of PS200 in dilute solution, measured by DLS for $c \simeq 0.01\%$. The values for TD are extrapolated from a temperature series of 30–50 °C.

Solvent	T_{bp}(°C)	T_m(°C)	ϕ_g	R_c (nm)
TD25	187	−31	0.46	31.8 ± 0.4
TD55	187	−31	0.30	51.0 ± 0.4
Toluene	110	−95	0.23	53.8 ± 0.3
Chloroform	61.2	−64	0.32	57.5 ± 0.2

which could arise from drawing the solution into a pipette and placing it onto the substrate prior to spinning. For all other solvents, films were formed at room temperature. After spin coating, all samples were annealed at 60 °C for 15 min to remove any residual solvent.

The experimental setup consisted of two nearly parallel plates that functioned as a plate capacitor. Polished silicon wafers were used as the negative electrodes onto which the PS films were spin-cast. Both silicon wafers and indium tin oxide coated glass slides were used as the positive electrodes. A small air gap was created between the plates using SU8 spacers deposited onto the positive electrode. The devices were placed into either a vacuum oven or a homemade, optically accessible, oven mounted on an inverted optical microscope, allowing for *in situ* observation of the instabilities, as described in Ref. [7]. The devices were assembled in the EHD setups at room temperature. The films were then heated to $T = 175\,°C > T_g$ and the temperature was allowed to equilibrate. The equilibration times were on the order of 5 and 20 min for the homemade and vacuum ovens, respectively. Once the temperature had equilibrated a voltage was applied to the two plates, defining the start of the experiment ($t = 0$). Films were used as-cast, after annealing at $T > T_g$ or after solvent vapor annealing. The plate spacing d was measured by atomic force microscopy after cooling the sample to room temperature and disassembling the capacitor device. A slight wedge geometry of the two plates (a variation of d of a few μm over a lateral distance of 1 cm) allowed the acquisition of data series with varying E_p on a single sample.

The setup used for solvent vapor annealing has been described in detail elsewhere [25]. The samples were placed into a chamber with a well-defined solvent vapor pressure. The saturation of the solvent vapor was controlled by using two streams of nitrogen gas, one of which was passed through a wash bottle filled with toluene, causing the toluene saturation of this stream. The two streams were mixed and introduced into the sample chamber. The flow rates of both streams were controlled by two electronic mass flow controllers. The precise adjustment of the relative flow rates controlled the relative solvent vapor pressure p/p_{sat} in fine increments from 0.00 to 1.00, which corresponds to a solvent vapor saturation from 0% to 100%. The temperatures of the solvent reservoir and the sample chamber were kept at the same temperature of 21 °C by separate temperature controllers.

The hydrodynamic radius R_c of PS200 (Table I) in the different solvents was measured using dynamic light scattering (DLS). The PS was dissolved into the different solvents to form dilute PS solutions with a concentration of $c = 0.01$wt% so that $c < c^*$, with c^* the overlap concentration. Each solution was filtered using a 0.1 μm PTFE filter into a standard glass cuvette, which was placed into a Malvern Zetasizer. Measurements for toluene and chloroform were carried out at 25 °C. A temperature series for TD yielded values for R_c of 33.7, 43.9, and 46.5 nm for 30,40, and 50 °C, respectively. Solutions were allowed to equilibrate for 5 min prior to the measurements. The hydrodynamic radius was determined by averaging ten experiments, with a standard error of less than 1%.

III. THEORETICAL DESCRIPTION

The physical principles underlying the destabilization of thin films by electric fields are well understood and have been described in detail elsewhere [26,27]. The formation of instabilities is determined by the dispersion relation, correlating the characteristic destabilization time τ with the wave vector q for each surface mode

$$\frac{1}{\tau} = -\frac{h_0^3}{3\eta}\left(\gamma q^4 + \frac{\partial p}{\partial h} q^2\right), \tag{1}$$

where γ is the surface tension, η is the viscosity, h_0 is the initial thickness of the film, h is the local film thickness, and p is the sum of all pressures, in addition to the Laplace pressure, acting at the liquid surface. The characteristic wavelength λ of the instabilities is given by the maximum of Eq. (1) and depends on the balance of pressures acting at the surface of the film such that

$$\lambda = 2\pi\sqrt{\frac{-2\gamma}{\partial p/\partial h}}. \tag{2}$$

Equation (2) reflects the balance of forces acting at the free interface and is independent of the film rheology.

For an ideal liquid film in the capacitor setup of Fig. 1 (inset), $p = p_{el}$ with

$$p_{el} = -\varepsilon_0 \varepsilon_p (\varepsilon_p - 1) E_p^2, \tag{3}$$

where ε_0 is the vacuum permittivity, ε_p is the dielectric constant of the polymer ($\varepsilon_{ps} = 2.5$), and $E_p = U(\varepsilon_p d - (\varepsilon_p - 1)h_0)^{-1}$ is the electric field in the polymer layer, d the capacitor plate spacing, and U the applied voltage. Substituting $p = p_{el}$ into Eq. (2) yields the characteristic instability wavelength

$$\lambda = 2\pi\sqrt{\frac{\gamma U}{\varepsilon_0 \varepsilon_p (\varepsilon_p - 1)^2}} E_p^{-\frac{3}{2}}. \tag{4}$$

Instabilities with a wavelength λ appear spontaneously after a characteristic onset time

$$\tau_D = \frac{3}{16\pi^4}\frac{\eta}{\gamma h_0^3}\lambda^4, \tag{5}$$

governed by the ratio of the film viscosity η to γ.

Equation (4) has been quantitatively validated [26]. Monitoring λ as a function of E_p can therefore test for additional contributions to p in Eq. (2). For spin-cast films such a contribution can arise from stresses in the film that result

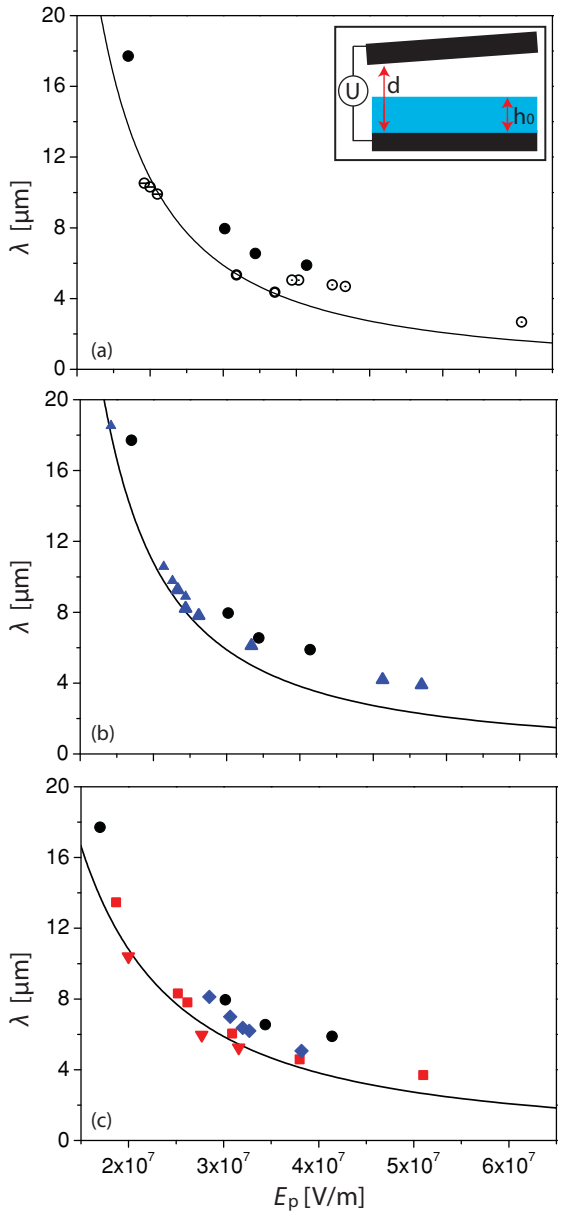

FIG. 1. (Color online) Characteristic instability wavelength λ of films spun from toluene as a function of the applied electric field E_p for (a) PS4000 (●) as-cast and films annealed for (⊙) 1 hour, (⊖) 10 hours, and (○) 140 hours at $T = 155\,^{\circ}$C. (b) As-cast films spun from toluene (●) PS4000 and (▲) PS200. (c) As-cast films spun from (♦) chloroform, (●) toluene, (■) TD55, and (▼) TD25. The line shows the prediction of Eq. (4). Experimental parameters: $h = 100$ nm, $U = 39.5$ V, $T = 175\,^{\circ}$C. The inset in (a) shows a schematic representation of the experimental setup.

from the preparation procedure. For spin-cast PS films, Eq. (5) measures the effective viscosity, which depends on the entangled nature of the polymer chains in the film [7].

IV. RESULTS

Two sets of experiments were performed. The first monitored the characteristic λ of the instabilities as a function of the applied electric field E_p, and the second measured the characteristic τ_D as a function of λ. This allowed the separate detection of stored residual stresses in the film and measurement of the rheological properties of the polymer chains. Films spun from the different solvents were destabilized directly after spin coating (as-spun films) and after annealing above T_g (annealed films).

Figure 1(a) shows the characteristic variation of λ for fully formed instabilities as a function of E_p for PS4000 films spun from toluene. The line is the prediction of Eq. (4). Each of the data points were acquired at a different lateral position on the same sample (the variation in E_p arose from a slight misalignment of the capacitor plates). Films annealed for 140 hours at 155 °C prior to destabilization are well described by this prediction. For as-cast films, however, all values of λ are systematically higher, with intermediate values observed for a film annealed for 1 hour.

A comparison of λ for as-cast films of PS4000 and PS200 is shown in Fig. 1(b). The deviation from the theoretical prediction is smaller for PS200 compared to PS4000. For both data sets the deviation is greater for large values of E_p and asymptotically approaches the solid line for $E_p \to 0$.

In Fig. 1(c), instabilities in PS4000 films cast from the different solvents listed in Table I are compared. Again, higher values of λ are observed for most as-cast films, but the degree of deviation from the predicted line varies with the casting solvent used. Comparing films spun from toluene and TD, Fig. 1(c) shows that the instabilities, which form in films prepared from TD, have smaller wavelengths than those prepared from toluene, with films spun from TD25 lying on the predicted line.

The onset times τ_D for EHD instabilities observed in PS200 films spun from toluene are shown in Fig. 2(a). Here τ_D is greatly reduced in the as-spun films compared to films annealed for 140 hours at 155 °C. Films annealed for intermediate times of 30, 70, and 96 hours have values of τ_D that lie between those of the as-spun and annealed films.

From Eq. (5), changes in τ_D may result from changes in γ and/or η. While surface tension is both temperature and molecular weight dependent [28], a variation in γ cannot account for the large decrease in τ_D demonstrated in Fig. 2(a) [7].

The derivation of Eq. (5) assumes a zero flow velocity of the polymer at the substrate. A reduction in τ_D is predicted if finite slip at the liquid-solid interface is taken into account in Eq. (5). It has previously been shown that the characteristic destabilization times are indistinguishable in films spun onto surfaces with differing surface energies [7]. This indicates that the solid boundary does not play a significant role during the early stage of destabilization.

The only likely parameter that can account for the decrease in τ_D is therefore the effective viscosity η. Fitting Eq. (5) to the annealed films gives an effective viscosity of 110 ± 5 kPa s, which corresponds closely to the bulk viscosity of the polymer [solid line Fig. 2(a)]. The dashed line in Fig. 2(a) shows a fit of Eq. (5) assuming an effective viscosity of 30 ± 2 kPa s, a factor of 4 below the bulk viscosity. Films annealed for 30, 70, and 96 hours have effective viscosities of 35 ± 2, 65 ± 5, and 90 ± 5 kPa s, respectively.

The data sets in Fig. 2(b) correspond to films spun from TD25, TD55, toluene, and chloroform. A clear difference in

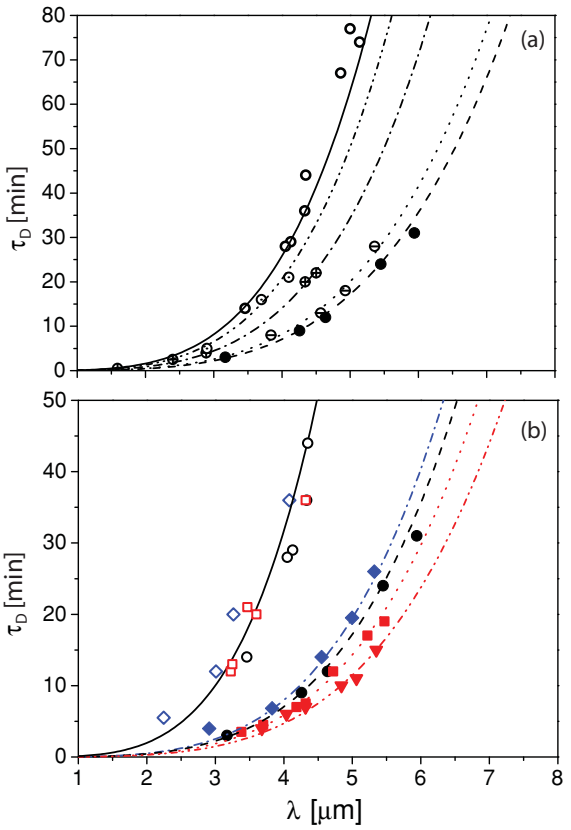

FIG. 2. (Color online) Characteristic destabilization time τ_D vs. λ for PS200. (a) Films spun from toluene (•) as-spun, after annealing at $T = 155\,^{\circ}$C for (⊖) 30 hours, (⊕) 70 hours, (⊙) 96 hours, and (○) 140 hours. (b) As-cast films spun from (▼) TD25 (■) TD55, and (♦) chloroform. Open symbols represent films annealed at $T = 155\,^{\circ}$C for 140 hours.

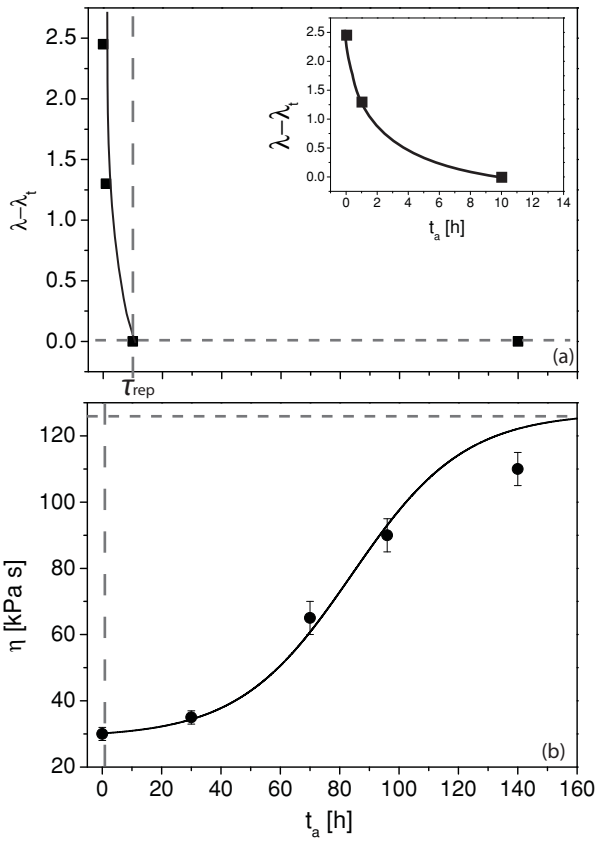

FIG. 3. Relaxation behavior of (a) residual stresses in PS4000 and (b) viscosity in PS200 as a function of the annealing time. The line is a fit to Eq. (6) with $\tau_\eta = 103$ hours. The vertical dashed lines indicate the reptation time. The horizontal dashed lines are the predictions of Eqs. (4) and (5) for fully equilibrated films.

τ_D is observed for films spun from the different solvents. The onset time is reduced in films spun from TD compared to films spun from toluene. For films cast from TD, τ_D depends on the temperature at which the films were prepared, with those spun at 55 °C (TD55) having a greater τ_D than those spun at 25 °C (TD25). Fitting the data gives the effective viscosities of TD25 and TD55 of 20 ± 2 and 25 ± 2 kPa s, respectively. Films spun from chloroform, on the other hand, show an increased effective viscosity of 34 ± 1 kPa s, as compared with those cast from toluene.

The variation of λ and τ_D with annealing time in Figs. 1(a) and 2(a) reflects the relaxation of the residual stress and effective viscosity, respectively. Figure 3(a) shows the variation in the instability wavelength from the value λ_t predicted by Eq. (4) for $E_p \approx 4 \times 10^7$ V/m. The change in the effective viscosity with time, shown in Fig. 3(b), was determined by fitting Eq. (5) to the data in Fig. 2(a). The annealing time required to remove the residual stresses in PS4000 is on the order of 10 hours, much shorter than the time needed to recover bulk viscosity [7].

The data trend of Fig. 3(b) suggests a sigmoidal variation. A sigmoid was therefore employed to empirically describe the data

$$\eta = \eta_0 + \frac{\eta_b - \eta_0}{1 + e^{-\frac{t-t_1}{t_2}}}, \qquad (6)$$

by varying t_1 and t_2. Here η_0 and η_b are the viscosities of the as cast films and the bulk, respectively. The characteristic relaxation time is defined as $\tau_\eta = t_1 + t_2$, corresponding to the point where $\approx 3/4$ of the bulk viscosity is recovered. For PS200 in Fig. 3(b), $\tau_\eta = 103$ hours.

V. DISCUSSION

A. Model

The results of Figs. 1 and 2 are interpreted in terms of the formation of nonequilibrium chain conformations caused by the evaporation of the solvent during film formation. Starting from a semidilute solution, the polymer concentration increases as the solvent evaporates. In order to maintain thermodynamic equilibrium, this requires a continuous increase of the entanglement density. An increase in polymer concentration, however, also increases the solution viscosity, slowing down the entanglement dynamics, which comes to a stop when the film vitrifies. Since film vitrification occurs at relatively high-solvent-volume fractions ϕ_g (Table I), chain conformations are frozen in semi-dilute conformations, which do not further equilibrate when the remaining solvent evaporates. This has consequences for the stored stresses and the rheological behavior of the resulting film, as discussed below.

B. Residual stresses

The values of λ for most of the as-cast films in Fig. 1 lie above the solid line. In terms of Eq. (4), an increase in λ indicates the presence of a stabilizing pressure $p_s < 0$ in addition to the destabilizing p_{el}: $p = p_{el} + p_s$. The results of Fig. 1 reveal the following trends: (1) $|p_s|$ increases with increasing molecular weight, (2) p_s depends strongly on the quality of the spin-casting solvent, and (3) the effect of p_s is more strongly pronounced for large values of E_p.

In-plane stresses caused by nonequilibrium chain conformations are well known and act to enhance hole formation and accelerate dewetting [22]. The enhanced hole formation driven by in-plane tensile stresses was explained by Vilmin and coworkers in terms of Eq. (2) [29]. While consistent with film dewetting, destabilizing in-plane stresses ($p_s > 0$) should give rise to *reduced* values of λ compared to the case where $p = p_{el}$ (solid lines in Fig. 1). Instead, an overall stabilizing effect of p_s is observed, validating earlier observations [7].

Despite the apparent contradiction with dewetting studies [22,29], the stabilizing effect observed here is likely to arise from frozen-in nonequilibrium chain conformations during film preparation. Qualitatively, the results of Fig. 1 suggest that the magnitude of p_s is governed by the coil dimensions at the vitrification point. In terms of Fig. 1(b), the swollen dimension of a PS4000 coil with a solvent content at the vitrification point ϕ_g is ∼6 times larger compared to PS200. The subsequent solvent evaporation therefore leads to a more strongly deformed oblate conformation of the higher molecular weight chains.

A similar effect is seen in terms of the solvent dependency of Fig. 1(c). While no measurable difference between as-cast and equilibrated TD25 films is found, the deviation increases for TD55, chloroform and toluene. Apart from the sequence of the chloroform and toluene data sets, the deviation from equilibrium behavior mirrors the trend in hydrodynamic chain dimensions R_c in Table I: The magnitude of the stabilizing p_s increases with increasing R_c and therefore with increasing solvent quality. Casting perfectly smooth films from chloroform is difficult because of the very low boiling point of chloroform, possibly explaining the inverted positions of the chloroform and toluene data.

Varying the solvent or the spin-coating temperature alters two additional parameters, which may play a role in the chain quenching process. First, the differing solvent melting points and spin-coating temperatures affect the vitrification point. The glass transition temperature of a polymer solution is given by Fox's equation [30]:

$$\frac{1}{T_{g_s}} = \frac{\phi_g}{T_m} + \frac{1-\phi_g}{T_g}, \tag{7}$$

where T_{g_s} is the glass transition temperature of the solution, T_m is the solvent melting temperature, and ϕ_g is the solvent volume fraction at which the film solidifies. Using tabulated values for T_m, $T_g \approx 105\,^\circ$C for PS, and $T_{g_s} = 55\,^\circ$C for TD55 and $T_{g_s} = 25\,^\circ$C for the other solvents, the solvent content at the vitrification point ϕ_g is calculated (Table I). In terms of the chain dimension at the vitrification point, larger deviations in the chain dimensions are expected for high values of ϕ_g, which is clearly not borne out by the data.

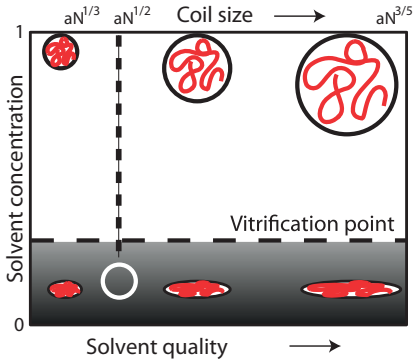

FIG. 4. (Color online) Schematic representation of polymer coil conformations upon spin coating for temperatures above and below the Θ temperature (vertical dashed line). The open circle indicates a fully entangled chain in equilibrium.

Second, the film formation kinetics may play a role. The drying time of the film during spin coating is governed by the boiling point of the solvent. Films form from chloroform in 1–3 seconds, from toluene in 5–10 seconds, and from TD in 30–45 seconds, with TD55 films forming slightly faster than those spun from TD25. A longer film formation time allows more time for the chains to equilibrate during the solvent evaporation process. While this contributes to the observed trend in the data, it is expected to be of minor importance [23].

The interplay of the effect of solvent quality and the vitrification point is schematically illustrated in Fig. 4. The boiling point of the solvent affects the speed with which a trajectory in Fig. 4 is traversed.

C. Effective viscosity

The arguments of the previous section not only lead to deformation of the chains, but also cause deviations in the entanglement density in the as-cast films. The entanglement density is essentially set by the number of interchain entanglements at the vitrification point. Interestingly, in terms of deviation from the equilibrated films, the series of the data sets in Fig. 2 is the inverse of Fig. 1(c), with TD25 showing the largest deviation from the equilibrated melt. This can again be understood in terms of the chain size and solvent content at the vitrification point, which fixes the number of interchain entanglements per coil in the quenched melt film. Near the Θ point (i.e., TD25), the chains in a semidilute solution are relatively compact and form few entanglements with neighboring chains compared to the highly swollen chains in an athermal solvent. This difference persists during solvent evaporation, leading to a difference in entanglement density at the vitrification point, with the strongest deviation from the equilibrated melt observed for the lowest quality spin-coating solvent. The variation of ϕ_g in Table I enhances this effect, with a higher solvent content at vitrification for TD25, compared to toluene and chloroform.

Differences in the molecular entanglements result in a substantial lowering of the polymer melt viscosity, which scales as $\eta \sim N_e^{-3.4}$, where N_e is the average number of monomers between interchain entanglements points. Low-quality casting solvents with high melting points therefore

result in the strongest lowering of the melt viscosity compared to the equilibrated film.

D. Evidence for "crust" formation?

The results of Figs. 1 and 2 are puzzling in two ways. The formation of oblate-shaped coils schematically shown in Fig. 4 suggests the buildup of an in-plane tensile stress, which should have a destabilizing effect on the film [20,22,23]. The results of Fig. 1 reveal a stabilizing effect, seemingly contradicting this model. Second, the results of Fig. 2 are interpreted in terms of a substantial lowering of the melt viscosity of the as-cast film, by several orders of magnitude for high-molecular-weight polymers [7]. It is surprising that such a substantial deviation from bulk rheology was not detected in earlier dewetting experiments.

It is therefore instructive to reexamine the experimental procedure used here. In contrast to dewetting experiments, where the motion of the contact line couples to the in-plane stress of the film, EHD experiments probe the force balance at the film surface, in the direction of the surface normal. Second, since the rheological analysis of Fig. 2 considers surface waves with amplitudes of ∼5 nm, the rheology of the only the surface-near layer is tested, rather than the film rheology as a whole. The differences of our extremely surface-sensitive measurements to other experiments may therefore arise from an abnormal structure of the chains in the surface-near layer of the film.

A possible mechanism for the formation of such surface-near layers has been suggested by de Gennes [31] and is shown in Fig. 5. When considering solvent evaporation from a drying film, de Gennes predicted the formation of a strongly nonlinear solvent volume fraction profile near the surface, with an effective width b. De Gennes argued that this "crust" layer turns glassy much more rapidly compared to the interior regions of the film. A rough argument predicts $b \sim 70$ nm, but since several of the parameters of the model are not well known, b might be smaller.

In the context of the present EHD experiments, the possible formation of such an altered surface-near region has interesting

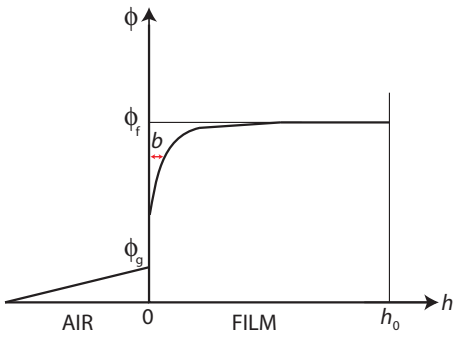

.

FIG. 5. (Color online) Schematic representation of the solvent volume fraction ϕ in the film and the adjacent air diffusion layer, predicted by de Gennes [31]. The nonlinear variation of ϕ leads to the rapid formation of a surface layer of width b with $\phi \approx \phi_g$, while the composition deeper in the film is $\phi_f > \phi_g$. The graph is adapted from Ref. [31].

consequences. In terms of Fig. 4, it is likely that the chains in this surface-near layer are even further from equilibrium than in the bulk of the film; that is, they are quenched to an even more oblate structure with fewer interchain entanglements. A more oblate chain conformation gives rise to higher in-plane stresses near the surface compared to the lower lying regions in the film. A more stressed surface region acts as a taught "membrane" over a less stressed matrix, giving rise to a restoring force opposing surface actuation. In terms of Eq. (2) the variation of the in-plane stresses with distance from the film surfaces results in a stabilizing $\partial p/\partial h$ component, explaining the results of Fig. 1. The lower number of chain entanglements near the surface should result in a lower effective surface viscosity, dominating the dynamic response of the EHD experiment.

While our experiments do not provide direct evidence for the nonlinear composition profile during spin coating and its consequences in terms of coil conformations, the crust model is in good qualitative agreement with our data, particularly in comparison with recent dewetting results.

E. Return to bulk behavior

The results of Fig. 3 show that the annealing time required to reach equilibrated film behavior depends on the measured observable. Deviations in the wavelength spectrum are annealed out after approximately one reptation time, while the recovery of equilibrium bulk rheology takes much longer. This suggests that stresses in the film can be removed over relatively short timescales. The recovery of bulk viscosity, however, requires complete reentanglement of the chains in the melt, which may take much longer. Similar to earlier findings [7] the recovery of bulk rheology for PS200 after ∼160 hours annealing is 5 orders of magnitude longer than the reptation time of ≈4 s at 175 °C. With a reptation time of ≈8 hours at 175 °C [32], the predicted rheological equilibration of PS4000 is extrapolated to one century. PS655 has an extrapolated equilibration time of ∼7 weeks.

These surprisingly long relaxation times are presently not understood but clearly arise from the quenched nature of the polymer coils during film formation. While the collapse of chains onto themselves by solvent removal below the vitrification point is likely to cause coil conformations far from equilibrium, it is not evident how this effects the reptation kinetics. Our results are in good agreement with other experimental observations that also report thin film equilibration kinetics in excess of the reptation time [13,16].

The extremely long relaxation times validate our experimental procedure. Since EHD measurements require the heating of the samples above T_g until the onset of the instability, the chains will partially equilibrate during the EHD experiment. These measurements are therefore only sensible when τ_D is smaller than the relevant relaxation time. The effect of chain equilibration is clearly visible in Fig. 1(b). For high values of E_p, the PS200 data deviate substantially from equilibrium λ values (solid line), approaching the solid line for $E_p \to 0$. Since $\tau_D \sim E_p^6$ [26], $E_p \to 0$ corresponds to increasingly long onset times for the instability, giving rise to partial equilibration of the chains. While this effect is discernible for the results shown in Fig. 1, it is negligible

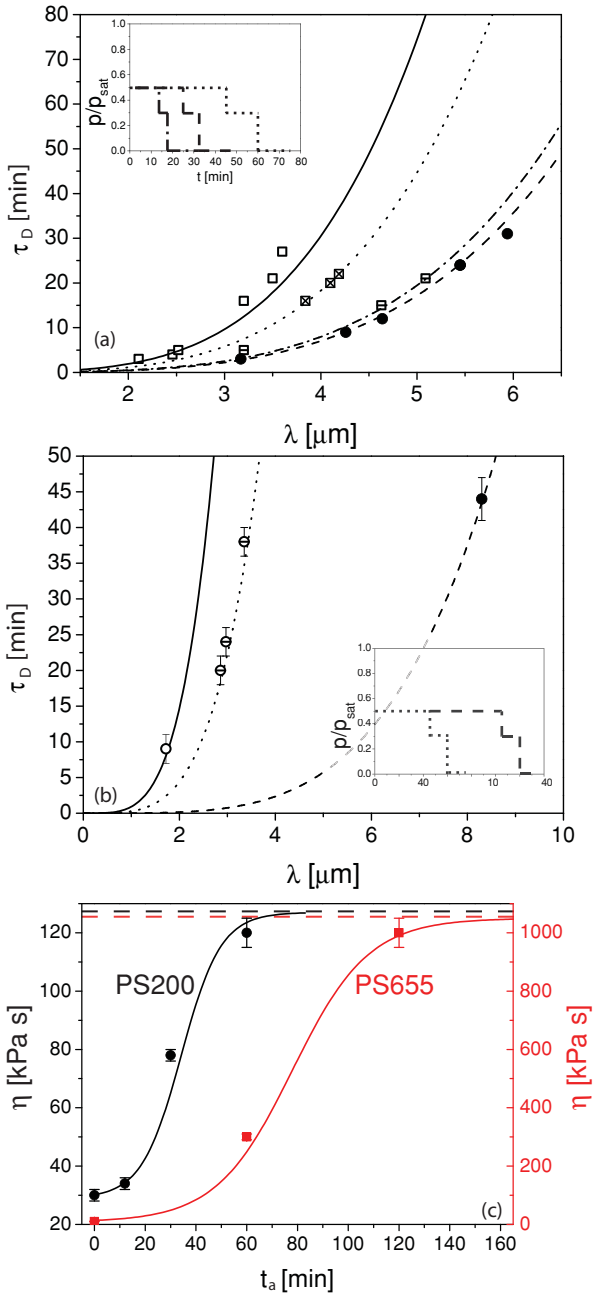

FIG. 6. (Color online) Characteristic destabilization τ_D vs. λ for vapor annealed films spun from (a) PS200 (•) as-spun, (⊟) t_a = 15 min, (⊠) t_a = 30 min, and (□) t_a = 60 min (b) PS655 (•) as-spun, (⊖) t_a = 60 min, and (○) t_a = 120 min. Insets show vapor annealing protocols. (c) Relaxation behavior of viscosity in (•) PS200 and (■) PS655. The lines are fits to Eq. (6) with τ_η = 42 min and τ_η = 93 min for PS200 and PS655, respectively.

for the τ_D measurements of Fig. 2, due to the much longer annealing times required for the recovery of the equilibrium viscosity.

The excessively long equilibration times of solvent-cast high-molecular-weight polymers raise the question whether such films can be equilibrated at all. Due to the high segmental friction parameter in the melt, the only feasible alternative to thermal annealing is solvent vapor annealing [33]. This involves the exposure of the polymer films to a well-controlled solvent-rich atmosphere, causing the swelling of the film at room temperature. Here PS200 films, spun from toluene, were annealed at 20 °C in a toluene atmosphere for a time t_a. The annealing protocol is shown in the insets of Fig. 6: the samples were kept at a vapor pressure of $p/p_{sat} = 0.5$ for $t_1 = 3/4\, t_a$ followed by a period of $t_2 = 1/4\, t_a$ at $p/p_{sat} = 0.3$. The films were then dried in a N_2 flow for 15 min.

Figure 6(a) shows the destabilization onset time for vapor annealed films for t_a = 15, 30, and 60 min. Solvent vapor annealing substantially accelerates film equilibration, as shown in Fig. 6(b). The lines in Figs. 3(b) and 6(c) are fits to Eq. (6). For PS200, τ_η decreases from 103 hours for thermally annealed films to 42 min when solvent vapor annealing was used. Solvent vapor annealing reduces equilibration of PS655 to a manageable 93 min, down from ∼7 weeks for thermal annealing.

VI. CONCLUSIONS

Polystyrene films of varying molecular weights cast from solvents of differing quality were examined by destabilization in an electric field. All films differed from the melt equilibrium in two ways: (1) film stability was increased, indicating the presence of a stabilizing surface pressure and (2) the onset time for the instabilities was substantially decreased, pointing to a lowered film viscosity. The variation of both effects as a function of the casting solvent can be explained in terms of the swollen coil size at the vitrification point, where the film has a solvent content of 20–50%. The collapse of the chains onto themselves during the evaporation of this residual solvent causes the uniaxial compression of the chains with a reduced number of interchain entanglements per chain. While this chain deformation should give rise to in-plane stresses, the entanglement reduction causes a reduction in the melt viscosity.

The trend seen in the data is qualitatively explained using the following model: The more compact chains cast from a near-Θ solution are less deformed and less entangled compared to film cast from an athermal solvent. The main discrepancy with a simple model that assumes a constant solvent-polymer composition across the film is the sign of the additional pressure acting on the film. While oblate chain deformations should give rise to destabilizing in-plane stresses, stabilizing pressures were observed in the EHD experiments. A strong vertical composition variation across the film, as proposed by de Gennes [31], leading to the formation of a surface-near layer with more strongly distorted chains during solvent evaporation, removes this contradiction. A more stressed and less entangled surface layer would account for both the observed increase in film stability and the vastly lowered effective viscosity measured with the EHD experiments.

Finally, the enormous thermal relaxation times required to reach films that display rheological equilibrium raises the question of whether high-molecular-weight films can be equilibrated at all. Annealing as-cast films in a well-controlled vapor atmosphere reduces the equilibration times of high-molecular-weight films to a few hours, down from several months of thermal annealing.

The understanding of the nature of the stresses in thin films, as well as their removal, paves the way for the manufacture of films in which these properties can be manipulated. This will provide a way not only to control (and possibly enhance) film stability, but also to better predict the various pattern formation mechanisms in thin films.

ACKNOWLEDGMENTS

We acknowledge useful discussions with Mithun Chowdhury and thank the EPSRC (EP/E022561 and PhD Plus) and the Deutsche Forschungsgemeinschaft (RE2273/3-1)for funding.

[1] J. Keddie, R. Jones, and R. Cory, Europhys. Lett. **27**, 59 (1994).
[2] M. Mukherjee, M. Bhattacharya, M. K. Sanyal, T. Geue, J. Grenzer, and U. Pietsch, Phys. Rev. E **66**, 061801 (2002).
[3] T. Miyazaki, K. Nishida, and T. Kanaya, Phys. Rev. E **69**, 022801 (2004).
[4] Z. Fakhraai, S. Valadkhan, and J. Forrest, Eur. Phys. J. E **18**, 143 (2005).
[5] H. Bodiguel and C. Fretigny, Phys. Rev. Lett. **97**, 266105 (2006).
[6] O. Tsui, Y. Wang, F. Lee, C.-H. Lam, and Z. Yang, Macromolecules **41**, 1465 (2008).
[7] D. R. Barbero and U. Steiner, Phys. Rev. Lett. **102**, 248303 (2009).
[8] S. Napolitano, A. Pilleri, P. Rolla, and M. Wübbenhorst, ACS Nano **4**, 841 (2010).
[9] J. E. Pye, K. A. Rohald, E. A. Baker, and C. B. Roth, Macromolecules **43**, 8296 (2010).
[10] H. Lu, W. Chen, and T. P. Russell, Macromolecules **42**, 9111 (2009).
[11] D. Mukherji and M. H. Muser, Phys. Rev. E **74**, 010601 (2006).
[12] Z. Jiang *et al.*, Phys. Rev. Lett. **98**, 227801 (2007).
[13] R. Jones, S. Kumar, D. Ho, R. Briber, and T. Russell, Nature (London) **400**, 146 (1999).
[14] J.-L. Masson and P. F. Green, Phys. Rev. E **65**, 031806 (2002).
[15] H. Kim, A. Rühm, L. B. Lurio, J. K. Basu, J. Lal, D. Lumma, S. G. J. Mochrie, and S. K. Sinha, Phys. Rev. Lett. **90**, 068302 (2003).
[16] H. Kim, A. Rühm, J. Lurio, L. B. Basu, J. Lal, S. Mochrie, and S. Sinha, J. Phys. Condens. Matter **16**, S3491 (2004).
[17] R. Seemann, S. Herminghaus, C. Neto, S. Schlagowski, D. Podzimek, R. Konrad, H. Mantz, and K. Jacobs, J. Phys. Condens. Matter **17**, S267 (2005).
[18] F. Ziebert and E. Raphaël, Phys. Rev. E **79**, 031605 (2009).
[19] G. Reiter, A. Al Akhrass, M. Hamieh, P. Damman, S. Gabriele, T. Vilmin, and E. Raphaël, Eur. Phys. T. Special Topics **166**, 165 (2009).
[20] T. Vilmin and E. Raphaël, Eur. Phys. J. E **21**, 161 (2006).
[21] P. Damman, S. Gabriele, S. Copée, S. Desprez, D. Villier, T. Vilmin, E. Raphaël, M. Hamieh, S. Al Akhrass, and G. Reiter, Phys. Rev. Lett. **99**, 036101 (2007).
[22] G. Reiter, M. Hamieh, P. Damman, S. Sclavons, S. Gabriele, T. Vilimin, and E. Raphaël, Nat. Mater. **4**, 754 (2005).
[23] A. Raegen, M. Chowdhury, C. Calers, A. Schmatulla, U. Steiner, and G. Reiter, Phys. Rev. Lett. **105**, 227801 (2010).
[24] J. Brandrup, E. Immergrut, and E. Grulke, eds., *Polymer Handbook*, 4th ed., Vols. 1 and 2 (Wiley Interscience, Hoboken, 1999).
[25] S. Hüttner, S. M, A. Chiche, G. Krausch, U. Steiner, and M. Thelakkat, Soft Matter **5**, 4206 (2009).
[26] E. Schäffer, T. Thurn-Albrecht, T. Russell, and U. Steiner, Europhys. Lett. **53**, 518 (2001).
[27] A. Onuki, Physica A **217**, 38 (1995).
[28] J. Moreira and N. Demarquette, J. Appl. Polym. Sci. **82**, 1907 (2001).
[29] T. Vilmin and E. Raphaël, Phys. Rev. Lett. **97**, 036105 (2006).
[30] H. Schneider, Macromol. Chem. **189**, 1941 (1988).
[31] P. de Gennes, Eur. Phys. J. E **7**, 31 (2002).
[32] A. Bach, K. Almdal, H. Rasmussen, and O. Hassanger, Macromolecules **36**, 5174 (2003).
[33] F. Doumenc, B. Guerrier, and C. Allain, Europhys. Lett. **76**, 630 (2006).